STRUCTURAL BIOLOGY COMMUNICATIONS

ISSN 2053-230X

Crystal structure of type II NADH:quinone oxidoreductase from *Caldalkalibacillus thermarum* with an improved resolution of 2.15 Å

Yoshio Nakatani,[a,b]* Wanting Jiao,[b,c,d] David Aragão,[e] Yosuke Shimaki,[a] Jessica Petri,[a,b] Emily J. Parker[b,c,d] and Gregory M. Cook[a,b]*

[a]Department of Microbiology and Immunology, University of Otago, 720 Cumberland Street, Dunedin 9054, New Zealand, [b]Maurice Wilkins Centre for Molecular Biodiscovery, The University of Auckland, Private Bag 92019, Auckland 1042, New Zealand, [c]Maurice Wilkins Centre for Molecular Biodiscovery, Biomolecular Interaction Centre, University of Canterbury, Christchurch, New Zealand, [d]Ferrier Research Institute, Victoria University of Wellington, Wellington, New Zealand, and [e]Australian Synchrotron, 800 Blackburn Road, Clayton 3168, Australia. *Correspondence e-mail: yoshio.nakatani@otago.ac.nz, gregory.cook@otago.ac.nz

Received 4 August 2017
Accepted 12 September 2017

Edited by R. L. Stanfield, The Scripps Research Institute, USA

Keywords: type II NADH:quinone oxidoreductase; NDH-2; respiratory enzymes; membrane proteins; quinone binding.

PDB reference: type II NADH dehydrogenase, 5wed

Supporting information: this article has supporting information at journals.iucr.org/f

Type II NADH:quinone oxidoreductase (NDH-2) is a respiratory enzyme found in the electron-transport chain of many species, with the exception of mammals. It is a 40–70 kDa single-subunit monotopic membrane protein that catalyses the oxidation of NADH and the reduction of quinone molecules *via* the cofactor FAD. NDH-2 is a promising new target for drug development given its essential role in many bacterial species and intracellular parasites. Only two bacterial NDH-2 structures have been reported and these structures are at moderate resolution (2.3–2.5 Å). In this communication, a new crystallization platform is reported that produced high-quality NDH-2 crystals that diffracted to high resolution (2.15 Å). The high-resolution NDH-2 structure was used for *in silico* quinone substrate-docking studies to investigate the binding poses of menadione and ubiquinone molecules. These studies revealed that a very limited number of molecular interactions occur at the quinone-binding site of NDH-2. Given that the conformation of the active site is well defined, this high-resolution structure is potentially suitable for *in silico* inhibitor-compound screening and ligand-docking applications.

1. Introduction

NADH:quinone oxidoreductase plays a central role in the transfer of electrons into the electron-transport chain for the generation of ATP, and in the maintenance of the cellular NAD^+/NADH redox balance. Three classes of respiratory NADH:quinone oxidoreductases, namely proton-pumping complex I, sodium-pumping NADH:quinone oxidoreductase and non-proton-translocating type II NADH:quinone oxidoreductase (NDH-2), have been identified in the respiratory chains of bacteria (Melo *et al.*, 2004; Kerscher *et al.*, 2008). NDH-2 is found in bacteria, fungi, yeast, protists and plants, but is absent in mammals (Melo *et al.*, 2004). NDH-2 is essential for the growth and survival of many human pathogens, including *Mycobacterium tuberculosis*, *Plasmodium falciparum* and *Toxoplasma gondii*, and has attracted attention for the development of new antitubercular and antiprotazoal agents (Biagini *et al.*, 2006; Saleh *et al.*, 2007; Griffin *et al.*, 2011; Weinstein *et al.*, 2005).

Both complex I and sodium-pumping NADH:quinone oxidoreductase form large multi-subunit membrane-protein complexes. They also have the ability to generate a membrane potential by translocating either protons or sodium ions across the membrane (Kerscher *et al.*, 2008; Melo *et al.*, 2004; Hirst, 2013). In contrast, NDH-2 is a 40–70 kDa monotopic

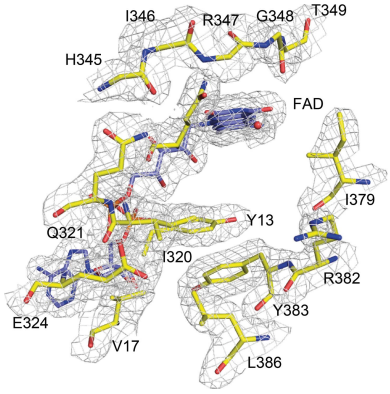

membrane protein that contains the cofactor FAD or FMN, and provides exergonic oxidation of NADH and reduction of quinone at two distinct substrate-binding sites. These binding sites are located on the *re* and *si* faces of the FAD isoalloxazine (Feng *et al.*, 2012; Sena *et al.*, 2015; Blaza *et al.*, 2017; Heikal *et al.*, 2014). NDH-2 does not have a proton-pumping function and may not directly support ATP synthesis by generating a proton-motive force. However, it supplies reduced quinones to terminal cytochrome oxidases and indirectly contributes to the generation of ATP.

To date, crystal structures of NDH-2 have been determined for only the following four species: *Saccharomyces cerevisiae* (Feng *et al.*, 2012; Iwata *et al.*, 2012), *Caldalkalibacillus thermarum* (Heikal *et al.*, 2014), *Staphylococcus aureus* (Sena *et al.*, 2015) and *P. falciparum* (Yang *et al.*, 2017). NDH-2 consists of three domains. Two are Rossmann folds, one holding the cofactor FAD and the other binding NADH. The third domain is a C-terminal membrane-anchoring domain that is enriched with both hydrophobic and positively charged amino-acid residues and binds NDH-2 to the phospholipid bilayer (Iwata *et al.*, 2012; Feng *et al.*, 2012; Heikal *et al.*, 2014). The quinone-binding site (Q-site) is located in this C-terminal domain. Some NDH-2 enzymes, such as that from *P. falciparum*, have a small additional domain (for example an EF-hand) between the second Rossmann fold and the membrane-anchoring domain, but the physiological function of this additional domain remains unknown (Yang *et al.*, 2017; Melo *et al.*, 2004). All of the reported NDH-2 structures have a homodimeric structure, but the functional significance of this remains unknown.

Over 4000 membrane-protein structures are available in the Protein Data Bank, but less than 22% of these structures have been determined at resolutions with numerical values lower than 2.0 Å (http://www.rcsb.org). High-resolution structures have been determined for the eukaryotic NDH-2 yeast Ndi1 (PDB entry 4g6h) at 2.26 Å resolution (Feng *et al.*, 2012) and *P. falciparum* PfNDH-2 (PDB entry 5jwc) at 2.05 Å resolution (Yang *et al.*, 2017). Reported bacterial NDH-2 structures are in the 2.3–2.5 Å resolution range (Sousa *et al.*, 2017; Heikal *et al.*, 2014). *In silico* compound screening and docking experiments are relatively easy to set up and do not require a large investment compared with conventional biochemical drug screening (Lagarde *et al.*, 2015). Notwithstanding this, successful application relies heavily on the quality of the scaffold protein structure (Lagarde *et al.*, 2015; Warren *et al.*, 2012). The crystal structure of a protein is not error-free, and coordination errors largely correlate with the resolution at which the structure is determined (Warren *et al.*, 2012). Ideally, the structure will have been determined with a high-quality data set (*i.e.* high resolution).

Previously, we reported a 2.5 Å resolution crystal structure of NDH-2 from the thermoalkaliphilic bacterium *C. thermarum* (Heikal *et al.*, 2014). In this study, we report a new crystallization platform that produced high-quality NDH-2 crystals resulting in a high-resolution (2.15 Å) bacterial NDH-2 structure. The high-resolution NDH-2 structure was used for *in silico* quinone substrate-docking studies to investigate the binding poses of menadione and ubiquinone molecules, which were predicted to adopt similar binding poses at the Q-site. The quinone head group is clamped by Glu317 and Ile379, and only one hydrogen bond forms to the N3 atom of the FAD isoalloxazine.

2. Materials and methods

2.1. NDH-2 protein expression and purification

NDH-2 from *C. thermarum* was expressed and purified as described previously (Heikal *et al.*, 2014).

2.2. Crystallization

The NDH-2 crystallization was performed using an established method (Heikal *et al.*, 2014), with modification of the conditions. We altered the original Morpheus crystallization buffer conditions (Gorrec, 2009), used a higher concentration of NDH-2 and used microseeding (Luft & DeTitta, 1999). The original buffer was 0.1 *M* Bicine/Tris pH 8.5 containing a mixture of 1,6-hexanediol, 1-butanol, 1,2-propanediol, 2-propanol, 1,4-butanediol and 1,3-propanediol (the final concentration of each component was 0.02 *M*), 10%(*v*/*v*) glycerol and 20%(*v*/*v*) polyethylene glycol 4000. The new buffer was 0.1 *M* Bicine/Tris buffer pH 8.5 containing 10%(*v*/*v*) polyethylene glycol 4000 and 25%(*v*/*v*) ethylene glycol. D,L-Lysine (30–150 m*M*) was added to the new buffer when required to slow the formation of crystals and to aid the growth of larger crystals. Dimethyl sulfoxide [DMSO; 1–7%(*v*/*v*)] was added when hydrophobic ligands were co-crystallized with NDH-2. For the crystal seeding stock, crystals were harvested in a Hampton Research seeding tube containing 100 µl of the new crystallization buffer excluding lysine. Stocks were prepared according to the manufacturer's instructions (Hampton Research, Aliso Viejo, California, USA). An NDH-2 sample with a concentration of 30 mg ml^{-1} was used for crystallization. Crystallization was performed using the hanging-drop vapour-diffusion method in 24-well plates, in which a drop containing 1 µl protein solution mixed with 1 µl precipitant buffer solution was set up against 1 ml reservoir solution. An aliquot (0.2 µl) of an appropriately diluted seeding stock was added immediately after mixing the protein and precipitant buffer solutions. Plates were incubated at 18°C and crystals formed immediately after seeding. The crystals were not harvested until day 4 to allow sufficient crystal growth to obtain high-quality crystals. Crystal quality rapidly deteriorated after day 7. It was serendipitously discovered that high-quality crystals that diffracted to beyond 2.3 Å resolution were produced with the addition of 1–10 m*M* menadione (MD) to the new buffer system. No additional cryoprotectant was required, and crystals were flash-cooled in liquid nitrogen for data collection.

2.3. Data collection and processing

The X-ray diffraction data were collected using a micro-focus beam at the Australian Synchrotron MX2 beamline. The detector distance was set to 300 mm. Each diffraction image

was collected with 30% beam attenuation and a 1° oscillation angle. Three data sets spanning 60, 90 and 60° were collected from a single crystal with 1.5, 2.0 and 2.5 s exposures, respectively. The data-collection point was moved each time to avoid radiation damage. All data sets were processed using the *XDS* package (Kabsch, 2010), and were merged and scaled using *AIMLESS* (Evans & Murshudov, 2013) in the *CCP*4 suite (Winn *et al.*, 2011). To minimize the introduction of model bias into the new structure, a polyalanine model was generated from chain *B* of PDB entry 4nwz (Heikal *et al.*, 2014) using *CHAINSAW* (Stein, 2008). Molecular replacement was performed using the *Phaser* crystallographic software with a polyalanine model (McCoy *et al.*, 2007). Structure refinement and manual modelling were carried out using *PHENIX* (Adams *et al.*, 2009) and *Coot* (Emsley *et al.*, 2010). *PyMOL* (Schrödinger) was used to create the figures. Data-collection and processing statistics are given in Table 1.

2.4. Molecular modelling of ubiquinone and MD in the Q-site

The structures of ubiquinone and MD were built in *Maestro* (Schrödinger) and then prepared for docking using *LigPrep* (Schrödinger). The Q-site in chain *B* of the new NDH-2 crystal structure was used for docking (Sastry *et al.*, 2013). The structure of NDH-2 was prepared using *Protein Preparation Wizard* (Schrödinger). Both ubiquinone and MD were then modelled in the Q-site using the induced-fit docking (Farid *et al.*, 2006; Sherman, Beard *et al.*, 2006; Sherman, Day *et al.*, 2006) protocol in the *Schrödinger Suite* (Schrödinger). The centre of the grid was defined as the centroid of residues 13, 44, 46, 47, 316, 317, 320, 347, 348, 349, 350, 376, 379, 380, 382 and 383. The side chains of residues 13, 347, 382 and 383 were trimmed off for initial docking. The van der Waals radii of the ligand and receptor atoms were scaled by a factor of 0.5. The top 20 poses from the initial docking were retained for optimization of the receptor residue conformations. Residues within a 5 Å distance of the respective docked ligand, with the exception of Glu317 and Glu321, were refined. The ligand was then re-docked into the top 20 newly generated receptor conformations that are within 30 kcal mol^{-1} of the best structure generated after refinement, using the extra-precision (XP) mode of *Glide* (Schrödinger).

3. Results and discussion

3.1. Production of high-quality NDH-2 crystals for improved resolution

We successfully established a new crystallization platform that consistently generated high-quality NDH-2 crystals that diffracted to beyond 2.5 Å resolution (20 out of 47 crystals tested). The original crystallization conditions used a mixture of volatile alcohols, which produced crystals that were difficult to handle. Consequently, the NDH-2 crystals were loosely packed and were sensitive to changes in the buffer conditions during crystal transfer. Most of the crystals obtained using the old buffer system diffracted to a resolution lower than 3.0 Å. Fortunately, we obtained one crystal that diffracted to 2.5 Å resolution in an earlier study (Heikal *et al.*, 2014). The fragility of the NDH-2 crystals was also evident in the number of failed ligand-soaking experiments that occurred using both the old and the new crystallization systems.

Table 1
Data-collection and refinement statistics for the high-resolution NDH-2 structure and comparison to the previously determined structure.

Values in parentheses are for the highest resolution shell.

	Higher resolution	Previous structure
Data-collection statistics		
Wavelength (Å)	0.954	0.954
Resolution (Å)	48.9–2.15 (2.19–2.15)	65.3–2.50 (2.64–2.50)
Space group	$P2_1$	$P2_1$
Unit-cell parameters		
a (Å)	72.8	72.8
b (Å)	113.6	114.5
c (Å)	129.8	130.6
β (°)	91.0	92.0
R_{merge}	0.092 (0.696)	0.060 (1.320)
$R_{p.i.m.}$	0.075 (0.610)	0.035 (0.761)
Mean $I/\sigma(I)$	17.3 (2.2)	15.8 (1.1)
Completeness (%)	91.9 (98.0)	99.6 (100.0)
Multiplicity	4.1 (3.1)	3.9 (4.0)
Total No. of reflections	428866 (17441)	290728 (43141)
No. of unique reflections	105403 (5541)	73752 (10759)
$CC_{1/2}$	0.982 (0.566)	0.999 (0.394)
Wilson B factor (Å^2)	38.6	76.0
Refinement statistics		
Resolution (Å)	48.9–2.15 (2.17–2.15)	64.6–2.50 (2.56–2.50)
R_{work}	0.208 (0.309)	0.217 (0.307)
R_{free}	0.238 (0.324)	0.269 (0.370)
R.m.s.d.s		
Bonds (Å)	0.003	0.010
Angles (°)	0.716	1.144
Chiral volume (Å^3)	0.003	0.07
No. of atoms		
Protein	11721	12029
Water	502	213
FAD	212	212
Average B factors (Å^2)		
Main chain	53.6	77.2
Side chain	56.0	83.7
Water	50.2	58.4
FAD	40.9	59.7
Ramachandran plot statistics (%)		
Favoured regions	98.1	96.8
Allowed regions	1.9	3.2
Outliers	0	0
PDB entry	5wed	4nwz

Compared with the old system, the new system was better for co-crystallization with both hydrophilic and hydrophobic ligands. Using this system, we previously determined the structure of an NAD$^+$–NDH-2 complex (Blaza *et al.*, 2017). Under the original conditions, no crystals formed in the presence of DMSO, which was added to solubilize highly hydrophobic NDH-2 substrates (*e.g.* quinones) and inhibitors. In contrast, with the new system we could use up to 7%(*v*/*v*) DMSO and still obtain NDH-2 crystals. In this study, we attempted to co-crystallize NDH-2 in the presence of 1,4-naphthoquinone, MD and several NDH-2 inhibitors (*e.g.* phenothiazines) that presumably bind at the Q-site. Although a number of crystals were obtained from the co-crystallization trials, none of the co-crystals had electron densities corresponding to these ligands either at the Q-site or at any other sites in the structure. However, we discovered that the

inclusion of 1–10 m*M* MD in the crystallization buffer produced many crystals that diffracted to beyond 2.3 Å resolution.

3.2. High-resolution structure of NDH-2

The 2.15 Å resolution structure of NDH-2 from *C. thermarum* was determined in space group $P2_1$, with unit-cell parameters a = 72.8, b = 113.6, c = 129.8 Å, β = 91°. These parameters were almost unchanged from those of the original 2.5 Å resolution structure (Table 1). After molecular replacement, four molecules were found in an asymmetric unit with well resolved electron density, allowing residues 3–396 to be built in all four chains. This is in contrast to the previous NDH-2 structure, in which the *D* chain was disordered compared with the other chains and some residues (83–90, 333–337 and 359–365) were missing (Heikal *et al.*, 2014). As described earlier, we did not observe additional electron density corresponding to MD in the structure.

The new structure improved the overall quality of the NDH-2 model. In the current model, more residues (98.1%) were built in the favoured regions of the Ramachandran plot than in the previous structure. The number of water molecules found in the new structure increased to approximately 500, which was 2.5 times that in the previous structure. The improved resolution was also evident in the lower average Wilson *B* factor and average *B* factor of the refined macromolecules and FAD ligands in the new structure, respectively (Table 1). In particular, the average Wilson *B* factor of the new data set decreased to 38.6 Å^2, which is approximately half that of the previously determined structure.

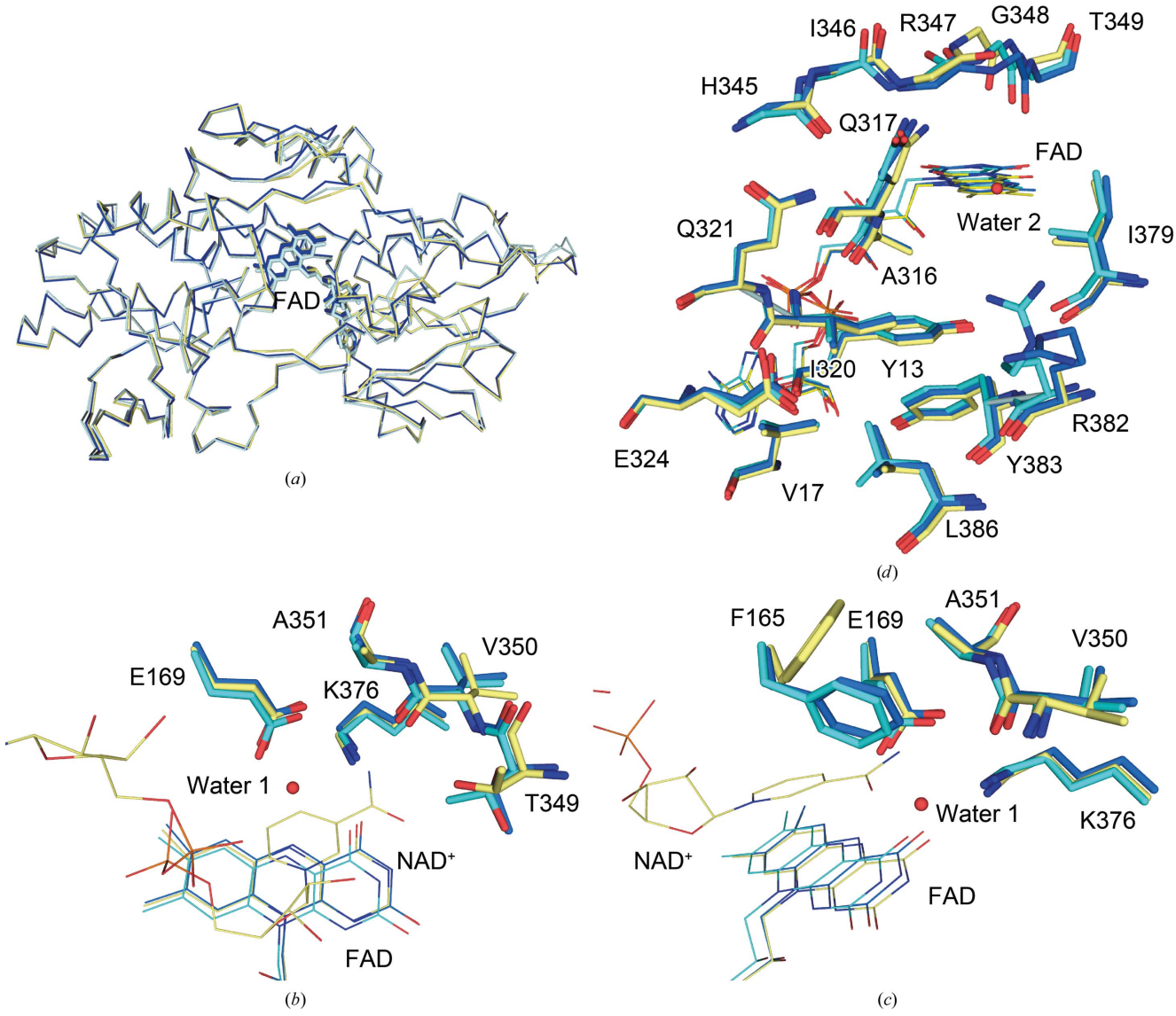

Figure 1
Comparison of the new (blue), old (PDB entry 4nwz; cyan) and NAD$^+$-bound (PDB entry 5kms; yellow) NDH-2 structures. (*a*) Superposition of the three structures. (*b*) Comparison with the nicotinamide-binding site. The identification codes for the NAD$^+$ molecule and the water molecule are PDB entries 5kms and 5wed, respectively. Phe165 is omitted for clarity. (*c*) A view of (*b*) rotated by 60° clockwise. Thr349 is omitted for clarity. (*d*) Comparison with the quinone-binding site. Side chains are omitted for residues 345–349 for clarity.

Among the four molecules in the asymmetric unit, the chain *B* molecule had the lowest average *B* factor (50.0 Å^2 for all atoms). Therefore, it was selected for subsequent structural analysis. For the same reason, chains *A* and *B* were used for a homodimer comparison. Overall, the wild-type structures from this study and our previous study did not differ significantly, with an r.m.s.d. of 0.526 Å over 392 C$^\alpha$ atoms (Fig. 1*a*). Their homodimeric structures were also comparable, with an r.m.s.d. of 0.766 Å over 784 C$^\alpha$ atoms. No noticeable structural differences were observed for the residues involved in the binding sites for NADH and quinone (Figs. 1*b*, 1*c* and 1*d*). Next, the high-resolution structure was compared with the structure of the NDH-2–NAD$^+$ complex (PDB entry 5kms; Blaza *et al.*, 2017). Again, overall, the two structures were comparable, with an r.m.s.d. of 0.407 over 394 C$^\alpha$ atoms. Only a couple of minor differences were noted at the nicotinamide binding site (Figs. 1*b* and 1*c*; Blaza *et al.*, 2017). These included minor structural rearrangements of the side chain of Thr349, with hydrogen-bond formation between its hydroxyl group and the nicotinamide O atom, and repositioning of the Phe165 side chain upon NADH binding. As expected, the two homodimers were very similar, with an r.m.s.d. of 0.440 Å over 788 C$^\alpha$ atoms, reconfirming that NAD(H) binding does not induce structural rearrangement in NDH-2.

3.3. Chemical geometries of the two substrate-binding sites

At 2.15 Å resolution, the electron density around the NDH-2 catalytic centre is well defined (Figs. 2*a* and 2*b*), providing a clear picture of atomic interactions at the active site of bacterial NDH-2. Residues Phe165, Glu169, Thr349–Ala351 and Lys376 are at the heart of the nicotinamide binding site on the *re* face of the FAD isoalloxazine (Figs. 2*c* and 2*d*). Previously, it has been shown that residues Phe165,

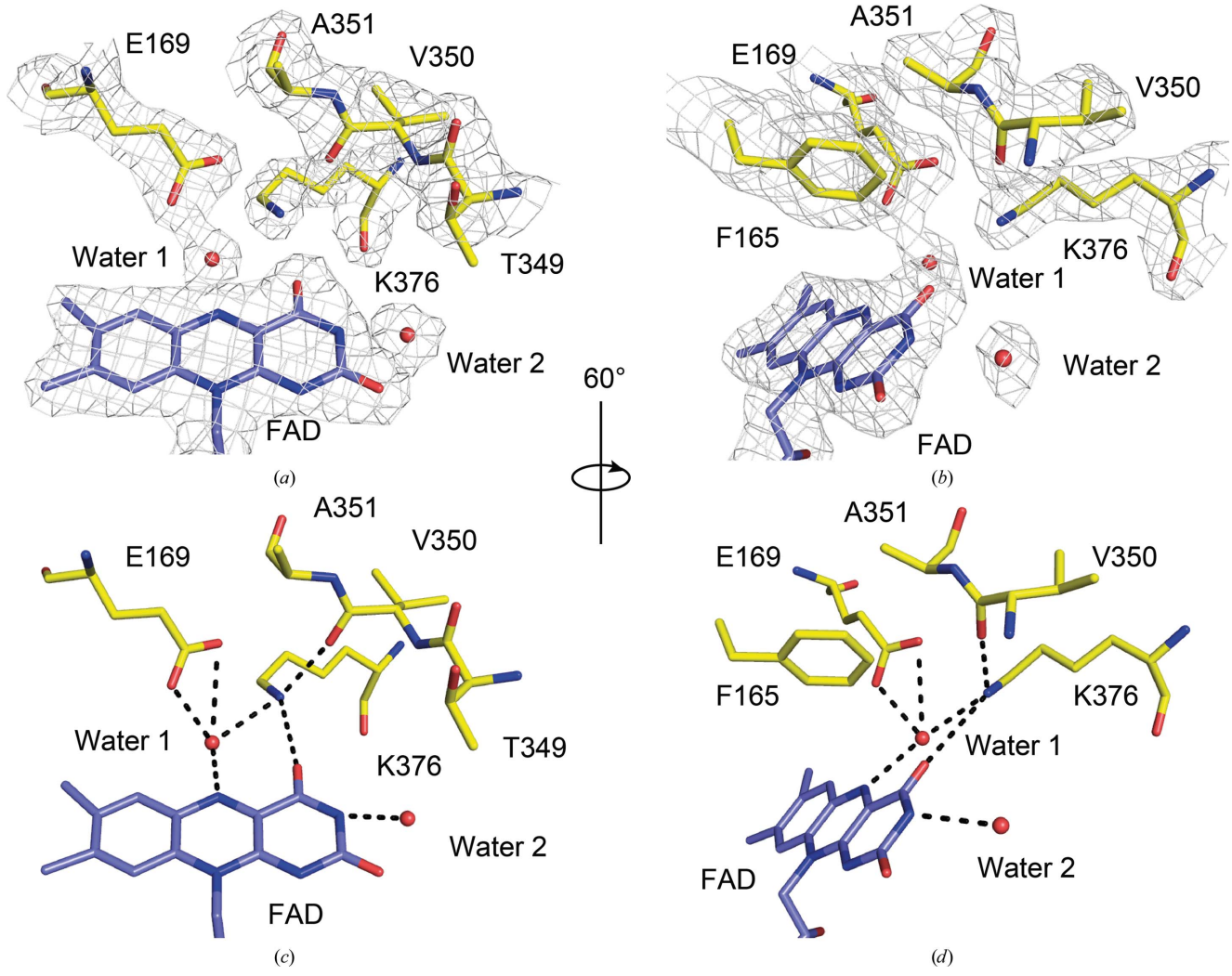

Figure 2
Nicotinamide-binding site of *C. thermarum* NDH-2. (*a*) A top view of the *re* face of the FAD isoalloxazine. The positions of both an FAD molecule (purple) and residues (yellow) involved in the nicotinamide-binding site are supported by an electron-density map shown as a grey mesh ($2F_o - F_c$ map contoured at 1σ). (*b*) A view of (*a*) rotated by 60° clockwise. (*c*) The same view as in (*a*) but without the electron-density map. (*d*) The same view as in (*b*) but without the electron-density map. Phe165 is omitted in (*a*) and (*c*) for clarity. Potential hydrogen-bonding interactions are shown by dashed lines in (*c*) and (*d*).

Thr349 and Val350 are directly involved in accommodating the nicotinamide group of NADH (Blaza *et al.*, 2017). Next, we looked at the Glu169 residue, which is a highly conserved residue in the NDH-2 family that potentially plays an important catalytic role in NADH oxidation in yeast Ndi1 (Feng *et al.*, 2012) and *S. aureus* NDH-2 (Marreiros *et al.*, 2017). In our structure, this residue firmly secured a water molecule (water 1) that resides next to the FAD ring (Fig. 2*c*). A relatively tight hydrogen bond formed between this water and the N5 atom of the isoalloxazine ring with a distance of 2.8 Å. Notably, in the previous structure this water was present in only two out of four chains and was loosely bonded to FAD (3.1–3.2 Å; Heikal *et al.*, 2014). An equivalent water molecule has been identified in the structure of yeast Ndi1 (PDB entry 4g6g; Feng *et al.*, 2012) but not in that of *P. falciparum* PfNDH-2 (PDB entry 5jwa; Yang *et al.*, 2017). Thus, the involvement of this water in catalysis remains unclear. It has been reported that a conserved mutation to an aspartate at the Glu242 residue of Ndi1, which is equivalent to Glu169 in NDH-2 from *C. thermarum*, causes a significant growth defect in *S. cerevisiae* (Feng *et al.*, 2012). This suggests that maintenance of the chemical environment, including the orientation of the glutamic acid side chain and water 1 at the *re* face of the FAD isoalloxazine, are important for NADH oxidation. The glutamic acid residue is highly conserved among all FAD-dependent reductases that use NADH or NADPH (Lee *et al.*, 2014; Marreiros *et al.*, 2017), and the orientation of the glutamate side chain and water 1 is likely to be a major determinant of whether the pK_a is optimal for NADH oxidation and FAD reduction. Finally, the new structure suggests that Lys376 plays an important role in stabilizing both the short linker separating the binding sites for NADH and quinone and the orientation of the FAD isoalloxazine. The ε-amino group of Lys376 hydrogen-bonds to a carbonyl O atom of Val350 and to the O4 atom of isoalloxazine. The *B* factor of the ε-amino N atom is 41.0 Å^2, which is the lowest among those of the residues shown in Figs. 2(*b*) and 2(*c*), which supports the proposed stabilization. This residue also coordinates to a water 1 molecule. In yeast Ndi1 (PDB entry 4g6g; Feng *et al.*, 2012) and *P. falciparum* PfNDH-2 (PDB entry 5jwa; Yang *et al.*, 2017) Lys376 is substituted by a tyrosine residue (Tyr482 and Tyr504) but plays the same role.

The electron density at the slot-shaped Q-site is also well defined. All residues and their side chains were unambiguously modelled (Figs. 3*a* and 3*b*). In the present structure, the previously proposed contacts between the Q-site motif AQ*X*A*X*Q (Heikal *et al.*, 2014; Marreiros *et al.*, 2016) and the short linker separating the two substrate-binding sites were confirmed with greater confidence. Hydrogen-bonding interactions between the main-chain atoms in the short linker and the two glutamine side chains were clearly supported by the electron-density maps (Figs. 3*a* and 3*b*). The *B* factors of the atoms involved in hydrogen bonding were lower than those of other atoms at the Q-site. The average *B* factor of the two O and N atoms of the two glutamate side chains was 50.4 Å^2, whereas the average *B* factor for the carboxyl O atoms and N atoms of the Glu324 and Arg382 side chains was 77.2 Å^2. The low *B* factor for the O and N atoms is further evidence of the hydrogen-bonding interactions. A well defined second water molecule (water 2) directly hydrogen-bonding to an N3 atom of the isoalloxazine was found at the Q-site (Figs. 2 and 3). In a similar manner to water 1, this water was present in only one chain in the previous structure but was present in all chains in the present structure. Interestingly, in the *in silico* quinone substrate modelling the positions of this water and the quinone carbonyl O atom overlapped (see §3.4).

3.4. Modelling of quinone substrates at the Q-site

Previously, we determined the crystal structure of NDH-2 complexed with NAD^+, but were unable to determine the structure of the quinone–substrate complex despite a number of attempts (Blaza *et al.*, 2017). The structure of yeast Ndi1 complexed with ubiquinone is the only structure that shows a physiologically relevant substrate bound at the Q-site of NDH-2 (Feng *et al.*, 2012). To understand how quinone molecules bind at the Q-site of the bacterial NDH-2 enzyme, we performed an *in silico* docking study based on the structure of the yeast Ndi1 complexed with ubiquinone (PDB entry 4g73; Feng *et al.*, 2012) and used it to model both the physiologically relevant substrate MD and a physiologically unrelated ubiquinone.

A lack of ligand/substrate presence in the Q-site of the bacterial NDH-2 crystal structure made it difficult to predict whether the conformations adopted by some residues (Arg347 and Arg382) were blocking the ubiquinone-binding pocket. Superposition of the Q-site between the bacterial NDH-2 crystal structure and yeast Ndi1 structure showed that residues Tyr13, Arg347, Arg382 and Tyr383 may block the binding pocket; therefore, the side chains of these residues were trimmed off for initial docking and then refined in our *in silico* modelling. In the yeast Ndi1 structure, binding of NADH or ubiquinone is not associated with conformational changes around two highly conserved glutamine residues (Gln317 and Gln321), which hydrogen-bond to the short linker separating the NADH-binding site and the Q-site (Feng *et al.*, 2012). Therefore, we assumed the same for our *in silico* quinone-docking experiments, and these hydrogen-bond contacts were maintained.

A ubiquinone molecule was comfortably placed in the Q-site of NDH-2 without major steric hindrance (Figs. 4*a* and 4*b*). The model showed that a ubiquinone head group nested into the hydrophobic slot-shaped Q-site, but with its carbon tail exposed to the solvent (Figs. 4*a* and 4*b*). The hydrophobic sections of the side chains of Gln317 and Ile379 held the planar quinone head. This observation is consistent with a previous study that showed that Ile379 is critical for quinone binding, and that any mutations greatly reduce its binding affinity (Blaza *et al.*, 2017). Only one hydrogen-bonding interaction was observed in the present model, with one of the carbonyl O atoms on the ubiquinone head hydrogen-bonding to the N5 atom of the cofactor FAD (Fig. 4*b*), as seen in the Ndi1–ubiquinone structure. Interestingly, the modelling program set this hydrogen-bond distance at 2.9 Å, which is

consistent with the hydrogen-bonding distance found between water 2 and the N3 atom of the isoalloxazine in the new crystal structure (Figs. 2 and 3). A molecule of water 2 observed in the Q-site potentially predicts the position of a quinone carbonyl O atom in the Q-site. No other specific interactions were observed between ubiquinone and NDH-2.

Similar to ubiquinone, MD was docked into the Q-site (Figs. 4*c* and 4*d*). Generally, MD adopts a very similar binding pose to that predicted for ubiquinone. The predicted pose contained two hydrogen bonds. As expected from the ubiquinone model, there was a hydrogen bond between MD and the FAD cofactor. The model showed that the other

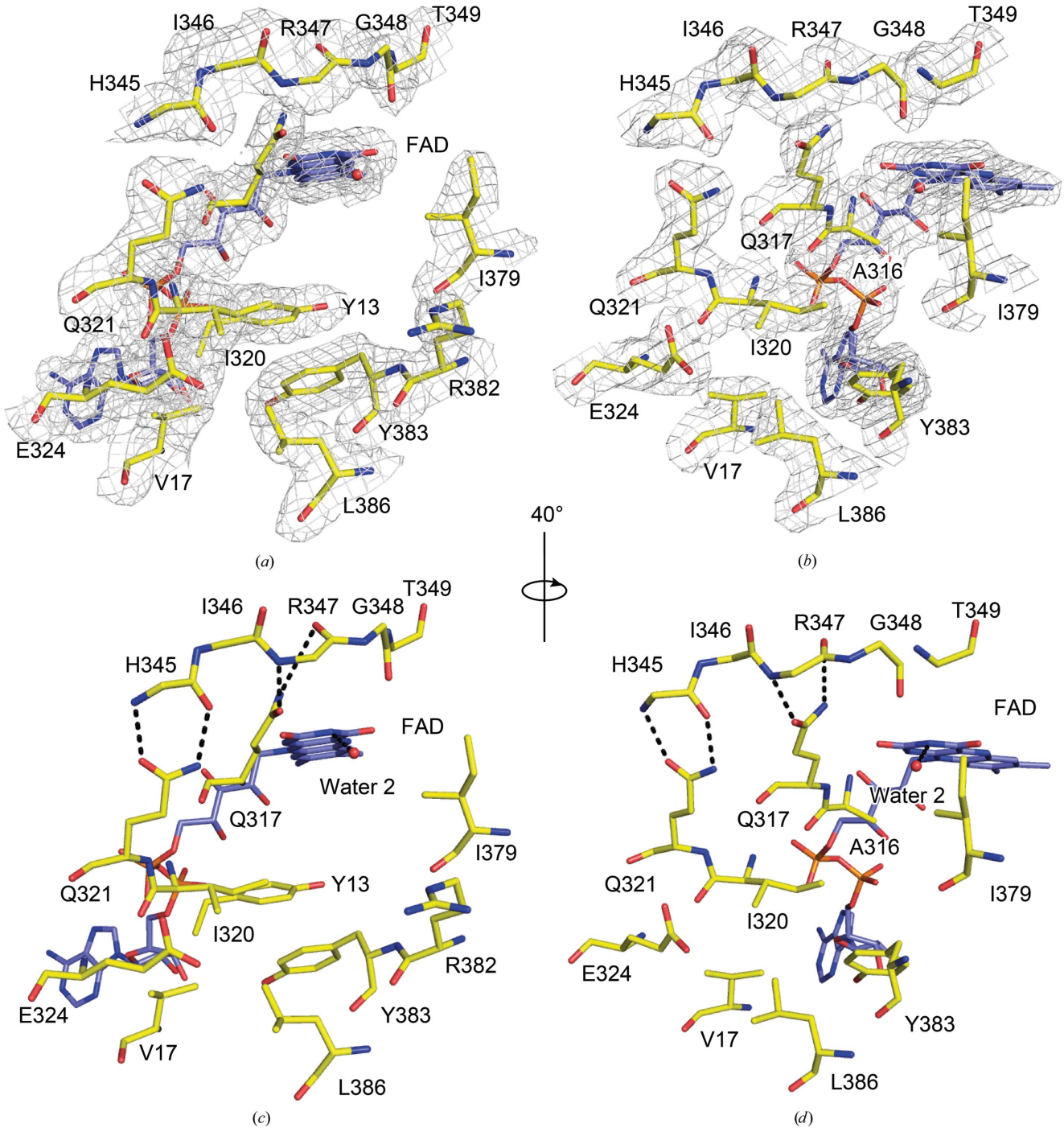

Figure 3
Quinone-binding site of *C. thermarum* NDH-2. (*a*) A quinone-binding site viewed from the *si* face of the FAD flavin ring. A $2F_o - F_c$ map contoured at 1σ is shown as a grey mesh. (*b*) A view of (*a*) rotated by 40° clockwise. (*c*) The same view as (*a*) but without the electron-density map. (*d*) The same view as (*b*) but without the electron-density map. Ala316 is omitted for clarity in (*a*) and (*c*). Arg382 is omitted in (*b*) and (*d*) for clarity. Potential hydrogen-bonding interactions are shown by dashed lines in (*c*) and (*d*).

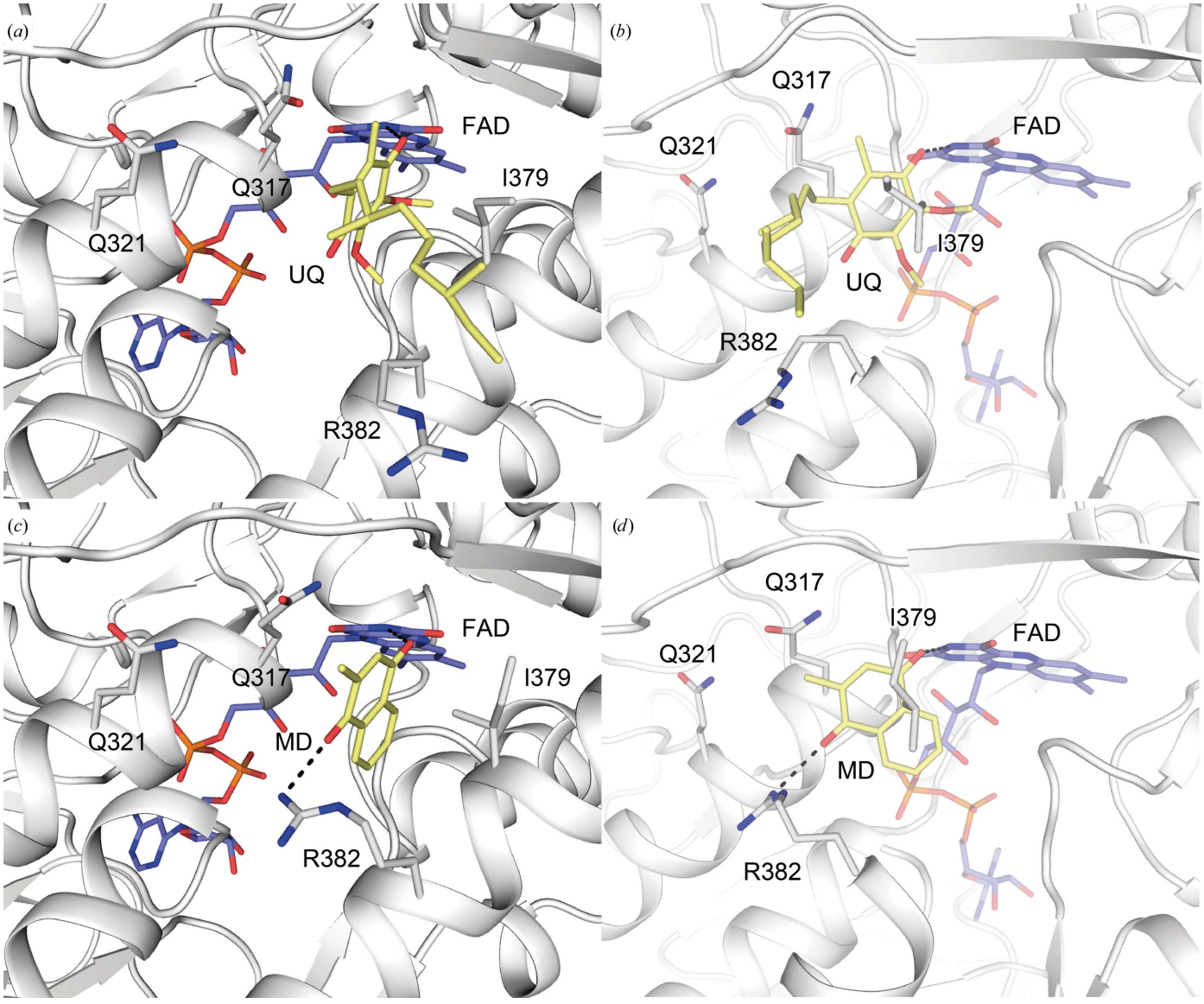

Figure 4
Ubiquinone and menadione docking at the quinone-binding site (Q-site) of NDH-2. (*a*) The docked ubiquinone in the Q-site, viewed from the *si* face of an FAD isoalloxazine. (*b*) A view of (*a*) rotated by 90° clockwise. (*c*) The docked menadione in the Q-site. (*d*) A view of (*c*) rotated by 90° clockwise. Potential hydrogen-bonding interactions are shown by dashed lines in (*b*) and (*d*).

ketone O atom of MD hydrogen-bonded to the side chain of Arg382. However, the significance of this contact remains unclear because the C-terminal membrane-anchoring domain containing the Q-site is presumably embedded in the membrane (Heikal *et al.*, 2014). This residue most likely preferably contacts a phosphate group of the phospholipid in the membrane-bound environment. It is worth mentioning that it appears that MD can bind deeper in the pocket than ubiquinone, presumably because of the lack of methyl ether groups on its quinone head. The aromatic ring of MD makes a distant edge-to-face π–π stacking with the FAD cofactor, which is not observed for ubiquinone. This additional chemical interaction might confer higher affinity than ubiquinone species, which is consistent with the fact that menaquinone is the sole quinone species found in *C. thermarum* (Kalamorz *et al.*, 2011). However, further experiments are required to prove this hypothesis.

4. Conclusions

We established a new crystallization platform to consistently produce high-quality NDH-2 crystals. Using these crystals, a high-resolution (2.15 Å) structure was determined for NDH-2. This platform will facilitate further crystallization of NDH-2 in the presence of both hydrophilic and hydrophobic ligands, which may ultimately contribute to the determination of substrate- and inhibitor-complex structures in the future. At 2.15 Å resolution, the molecular architecture, including water molecules at the two substrate-binding sites, was defined with confidence. Therefore, this high-resolution structure will be

suitable for *in silico* screening and docking of inhibitors. Finally, we performed *in silico* MD and ubiquinone docking. These compounds adopt similar binding poses at the Q-site, with the only interactions occurring between the quinone head group and residues Gln317 and Ile379, and the N3 atom of the FAD isoalloxazine. Both the new co-crystallization platform and the *in silico* template model could be applied to determination of NDH-2–inhibitor complex structures, which is a step towards the rational development of new inhibitors for drug development.

Acknowledgements

We thank Gabrielle David PhD for editing a draft of this manuscript. Author contributions are as follows. YN, JP and YS expressed, purified and crystallized the protein. YN and DA solved the crystal structure. WJ performed the *in silico* docking studies. YN, WJ, EJP and GMC analysed the data and wrote the manuscript, with help from the other authors. YN, WJ, EJP and GMC designed the research and directed the project. The authors declare no competing financial interests.

Funding information

This work was funded by the Maurice Wilkins Centre for Molecular Biodiscovery and the Health Research Council of New Zealand.

References

Adams, P. D., Mustyakimov, M., Afonine, P. V. & Langan, P. (2009). *Acta Cryst.* D**65**, 567–573.
Biagini, G. A., Viriyavejakul, P., O'Neill, P. M., Bray, P. G. & Ward, S. A. (2006). *Antimicrob. Agents Chemother.* **50**, 1841–1851.
Blaza, J. N., Bridges, H. R., Aragão, D., Dunn, E. A., Heikal, A., Cook, G. M., Nakatani, Y. & Hirst, J. (2017). *Sci. Rep.* **7**, 40165.
Emsley, P., Lohkamp, B., Scott, W. G. & Cowtan, K. (2010). *Acta Cryst.* D**66**, 486–501.
Evans, P. R. & Murshudov, G. N. (2013). *Acta Cryst.* D**69**, 1204–1214.
Farid, R., Day, T., Friesner, R. A. & Pearlstein, R. A. (2006). *Bioorg. Med. Chem.* **14**, 3160–3173.
Feng, Y., Li, W., Li, J., Wang, J., Ge, J., Xu, D., Liu, Y., Wu, K., Zeng, Q., Wu, J.-W., Tian, C., Zhou, B. & Yang, M. (2012). *Nature (London)*, **491**, 478–482.
Gorrec, F. (2009). *J. Appl. Cryst.* **42**, 1035–1042.
Griffin, J. E., Gawronski, J. D., Dejesus, M. A., Ioerger, T. R., Akerley, B. J. & Sassetti, C. M. (2011). *PLoS Pathog.* **7**, e1002251.
Heikal, A., Nakatani, Y., Dunn, E., Weimar, M. R., Day, C. L., Baker, E. N., Lott, J. S., Sazanov, L. A. & Cook, G. M. (2014). *Mol. Microbiol.* **91**, 950–964.
Hirst, J. (2013). *Annu. Rev. Biochem.* **82**, 551–575.
Iwata, M., Lee, Y., Yamashita, T., Yagi, T., Iwata, S., Cameron, A. D. & Maher, M. J. (2012). *Proc. Natl. Acad. Sci. USA*, **109**, 15247–15252.
Kabsch, W. (2010). *Acta Cryst.* D**66**, 125–132.
Kalamorz, F. *et al.* (2011). *J. Bacteriol.* **193**, 4290–4291.
Kerscher, S., Dröse, S., Zickermann, V. & Brandt, U. (2008). *Results Probl. Cell Differ.* **45**, 185–222.
Lagarde, N., Zagury, J.-F. & Montes, M. (2015). *J. Chem. Inf. Model.* **55**, 1297–1307.
Lee, K. H., Humbarger, S., Bahnvadia, R., Sazinsky, M. H. & Crane, E. J. III (2014). *Biochim. Biophys. Acta*, **1844**, 1708–1717.
Luft, J. R. & DeTitta, G. T. (1999). *Acta Cryst.* D**55**, 988–993.
Marreiros, B. C., Sena, F. V., Sousa, F. M., Batista, A. P. & Pereira, M. M. (2016). *Environ. Microbiol.* **18**, 4697–4709.
Marreiros, B. C., Sena, F. V., Sousa, F. M., Oliveira, A. S. F., Soares, C. M., Batista, A. P. & Pereira, M. M. (2017). *Sci. Rep.* **7**, 42303.
McCoy, A. J., Grosse-Kunstleve, R. W., Adams, P. D., Winn, M. D., Storoni, L. C. & Read, R. J. (2007). *J. Appl. Cryst.* **40**, 658–674.
Melo, A. M. P., Bandeiras, T. M. & Teixeira, M. (2004). *Microbiol. Mol. Biol. Rev.* **68**, 603–616.
Saleh, A., Friesen, J., Baumeister, S., Gross, U. & Bohne, W. (2007). *Antimicrob. Agents Chemother.* **51**, 1217–1222.
Sastry, G. M., Adzhigirey, M., Day, T., Annabhimoju, R. & Sherman, W. (2013). *J. Comput. Aided Mol. Des.* **27**, 221–234.
Sena, F. V., Batista, A. P., Catarino, T., Brito, J. A., Archer, M., Viertler, M., Madl, T., Cabrita, E. J. & Pereira, M. M. (2015). *Mol. Microbiol.* **98**, 272–288.
Sherman, W., Beard, H. S. & Farid, R. (2006). *Chem. Biol. Drug Des.* **67**, 83–84.
Sherman, W., Day, T., Jacobson, M. P., Friesner, R. A. & Farid, R. (2006). *J. Med. Chem.* **49**, 534–553.
Sousa, F. M., Sena, F. V., Batista, A. P., Athayde, D., Brito, J. A., Archer, M., Oliveira, S. F., Soares, C. M., Catarino, T. & Pereira, M. M. (2017). *Biochim. Biophys. Acta*, **1858**, 823–832.
Stein, N. (2008). *J. Appl. Cryst.* **41**, 641–643.
Warren, G. L., Do, T. D., Kelley, B. P., Nicholls, A. & Warren, S. D. (2012). *Drug Discov. Today*, **17**, 1270–1281.
Weinstein, E. A., Yano, T., Li, L.-S., Avarbock, D., Avarbock, A., Helm, D., McColm, A. A., Duncan, K., Lonsdale, J. T. & Rubin, H. (2005). *Proc. Natl. Acad. Sci. USA*, **102**, 4548–4553.
Winn, M. D. *et al.* (2011). *Acta Cryst.* D**67**, 235–242.
Yang, Y., Yu, Y., Li, X., Li, J., Wu, Y., Yu, J., Ge, J., Huang, Z., Jiang, L., Rao, Y. & Yang, M. (2017). *J. Med. Chem.* **60**, 1994–2005.